Charge Transfer at the $Ni_3InN/SrVO_3$ Heterointerfaces

Ting Cui(崔婷)[1,2†], Ying Zhou(周颖)[3†], Qinghua Zhang(张庆华)[1], Qianying Wang(王倩英)[1,2], Dongke Rong(荣东珂)[1,2], Haitao Hong(洪海涛)[1,2], Songhee Choi[1], Axin Xie(谢阿新)[1,2], Jun-Jie Zhang(张骏杰)[3], Can Wang(王灿)[1,2], Chen Ge(葛琛)[1,2], Lin Gu(谷林)[4], Shanmin Wang(王善民)[5], Kuijuan Jin(金奎娟)[1,2*], Shuai Dong(董帅)[3*], and Er-Jia Guo(郭尔佳)[1,2*]

[1]*Beijing National Laboratory for Condensed Matter Physics and Institute of Physics, Chinese Academy of Sciences, Beijing 100190, China*
[2]*Department of Physics & Center of Materials Science and Optoelectronics Engineering, University of Chinese Academy of Sciences, Beijing 100049, China*
[3]*Key Laboratory of Quantum Materials and Devices of Ministry of Education, School of Physics, Southeast University, Nanjing 211189, China*
[4]*National Center for Electron Microscopy in Beijing and School of Materials Science and Engineering, Tsinghua University, Beijing 100084, China*
[5]*Department of Physics, Southern University of Science and Technology, Shenzhen 518055, China*

(Received 20 August 2025; accepted manuscript online 27 August 2025)

Heterointerfaces have been pivotal in unveiling extraordinary interfacial properties and enabling multifunctional material platforms. Despite extensive research on all-oxide interfaces, heterointerfaces between different material classes, such as oxides and nitrides, remain underexplored. Here we present the fabrication of atomically sharp heterointerfaces between antiperovskite Ni_3InN and perovskite $SrVO_3$. Leveraging layer-resolved scanning transmission electron microscopy and electron energy loss spectroscopy, we identified pronounced charge transfer across the well-ordered interface. First-principles calculations confirmed our experimental observations and further predicted an emergent magnetic moment within the Ni_3InN layer due to the charge transfer. These findings pave the way for novel electronic and spintronic applications by enabling tunable interfacial properties in nitride/oxide systems.

DOI: 10.1088/0256-307X/42/10/100705 CSTR: 32039.14.0256-307X.42.10.100705

1. Introduction. Heterointerfaces are a fundamental aspect of modern materials science, enabling the discovery of emergent phenomena arising from the interaction of distinct material properties. Two-dimensional electron gas,[1,2] polar metal,[3] strong polarization enhancement,[4,5] unexpected magnetic anisotropy,[6,7] and exchange bias,[8–10] have been discovered over decades. In the past, research has primarily focused on heterointerfaces between two oxides or two semiconductors, while the exploration of other innovative interface systems has been relatively limited. Advances in thin-film growth techniques now allow for the precise fabrication of high-crystallinity nitrides, facilitating the creation of nitride/oxide heterointerfaces.[11–13]

Recently, nitride/oxide interfaces represent an exciting frontier, combining the robustness and high-performance characteristics of nitrides with the functional diversity of oxides. Previous work by Jin *et al.*[12] demonstrates the room-temperature ferromagnetism observed at the interface composed of an antiferromagnetic CrN and an antiferromagnetic Cr_2O_3. Except for the binary nitrides with simple crystal structures, ternary nitrides, especially antiperovskite-type nitrides, are known for their exceptional electronic and thermal properties.[14–20] More importantly, the structures of antiperovskite nitrides resemble those of perovskites, with the cation and anion positions swapped, sharing a similar crystal structure and lattice constants as most perovskite oxides, enabling heterogeneity between these two classes of materials at an atomic-scale interface.[21] Therefore, this type of heterointerface holds promise for discovering novel electronic, magnetic, and optical behaviors, particularly in the realm of quantum materials.[17,22]

Interfacial charge transfer is a key phenomenon at the heterointerfaces, where electron redistribution occurs due to differences in electronic structure and chemical potential.[23–28] This phenomenon often gives rise to unexpected and emergent properties, including interfacial conductivity,[29,30] magnetism,[31] and topological states.[32] However, when charge transfer occurs in systems with strong electron correlations, as in the case of many oxides,[33–36] the dynamics become highly complex. In nitride/oxide interfaces, these challenges are amplified by stark differences in bonding nature, orbital hybridization,

†These authors contributed equally to this work.
*Corresponding authors. Email: kjjin@iphy.ac.cn; sdong@seu.edu.cn; ejguo@iphy.ac.cn
© 2025 Chinese Physical Society and IOP Publishing Ltd. All rights, including for text and data mining, AI training, and similar technologies, are reserved.

and chemical environments. As a result, charge carrier migration across the interface can profoundly influence the overall functionality of these heterostructures. Addressing these challenges requires an integrated approach, combining advanced synthesis techniques with atomic-scale characterization and theoretical modeling.

In this work, we constructed the heterointerface between metallic antiperovskite Ni_3InN and correlated metallic perovskite $SrVO_3$. Utilizing a combination of layer-resolved scanning transmission electron microscopy (STEM) and electron energy loss spectroscopy (EELS), we systematically examine the interfacial charge transfer behavior across the interfaces. First-principles calculations are employed to elucidate the microscopic origin of interfacial charge transfer and its influence on the system's electronic and magnetic properties.

2. Synthesis and Characterization of $Ni_3InN/SrVO_3$ Bilayers. We selected antiperovskite Ni_3InN as our model system. Ni_3InN is theoretically predicted to be a Dirac metal, exhibiting ultrahigh conductivity due to its linear band dispersion near the Fermi level. $SrVO_3$ (∼3.84 Å, $Pm\bar{3}m$),[37] with a lattice constant closely matching that of Ni_3InN (∼3.84 Å, $Pm\bar{3}m$),[38] is expected to form high-quality coherent heterointerfaces [Fig. 1(a)]. Another advantage of $SrVO_3$ is that it can be grown with high crystalline quality under vacuum conditions compatible with those required for Ni_3InN. To construct the heterostructure, we first deposited a 10-nm-thick $SrVO_3$ film on (001)-oriented $(La_{0.3}Sr_{0.7})(Al_{0.65}Ta_{0.35})O_3$ (LSAT) substrates by pulsed laser deposition. The deposition was carried out with a laser fluence of ∼1 J·cm^{-2} and a substrate temperature of 500 °C, parameters optimized to promote epitaxial growth. On top of this buffer layer, a 10-nm-thick Ni_3InN film was subsequently deposited under the identical conditions. All growth processes were performed in vacuum to minimize undesirable oxidation and ensure sharp, coherent interfaces. The film thicknesses were estimated by counting laser pulses.

Figure 1(b) shows XRD θ–2θ scans of $Ni_3InN/SrVO_3$ bilayers, confirming the single-phase nature of both layers as evidenced by the observation of only (00l) reflections. Phi scans and reciprocal space mapping (RSM) analysis show the (113) reflections of both Ni_3InN and $SrVO_3$ around LSAT substrates [inset of Fig. 1(b) and Fig. 1(c)]. The results confirm the fourfold crystal symmetry of the thin films and the cube-on-cube epitaxial relationship with the substrates. Notably, we observed an apparent discrepancy in the relative diffraction intensities: the (002) reflection of $SrVO_3$ exhibits a stronger intensity than that of Ni_3InN, whereas the (113) reflection of $SrVO_3$ is weaker compared to that of Ni_3InN. To clarify this, we examined the powder diffraction patterns of both materials and found that, indeed, the intrinsic intensity of the $SrVO_3$ (113) reflection is lower than that of Ni_3InN, consistent with our observations. We performed high-angle annular dark field (HAADF) imaging and EELS mapping using STEM to verify the epitaxial growth and chemical distribution across the $Ni_3InN/SrVO_3$ interfaces. Figure 1(d) presents a representative HAADF image of the $Ni_3InN/SrVO_3$ interface along the [100] orientation. In HAADF imaging, the atomic column intensity scales approximately with the atomic number, such that the brighter contrast corresponds to $SrVO_3$, while the darker region corresponds to Ni_3InN.

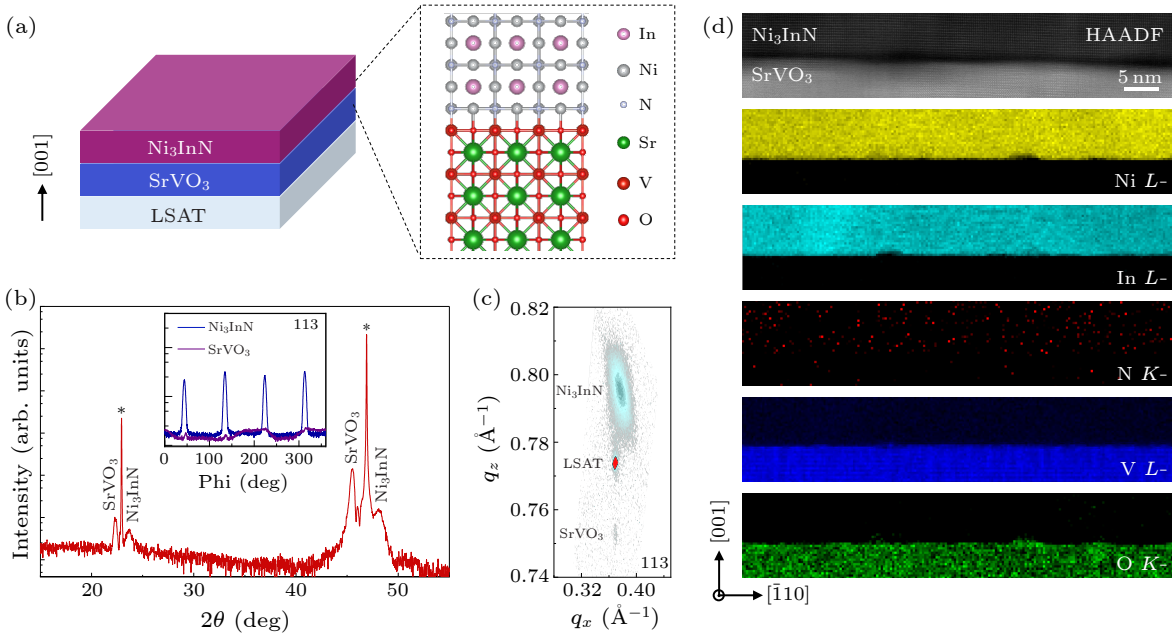

Fig. 1. Structural characterizations and chemical distribution of $Ni_3InN/SrVO_3$ heterointerface. (a) Sample geometry and schematic of heterointerfaces. (b) XRD θ–2θ scans of $Ni_3InN/SrVO_3$ bilayer on LSAT substrates (indicated with *). The inset presents Phi scans of the Ni_3InN and $SrVO_3$ films around the 113 reflections, confirming the fourfold symmetry of Ni_3InN and $SrVO_3$. (c) RSM of an Ni_3InN single layer around the substrate's 113 reflection, providing insights into lattice coherence and strain. (d) HAADF-STEM image of $Ni_3InN/SrVO_3$ heterostructure and compositional EELS mappings at Ni L-, In L-, N K-, V L-, and O K-edges.

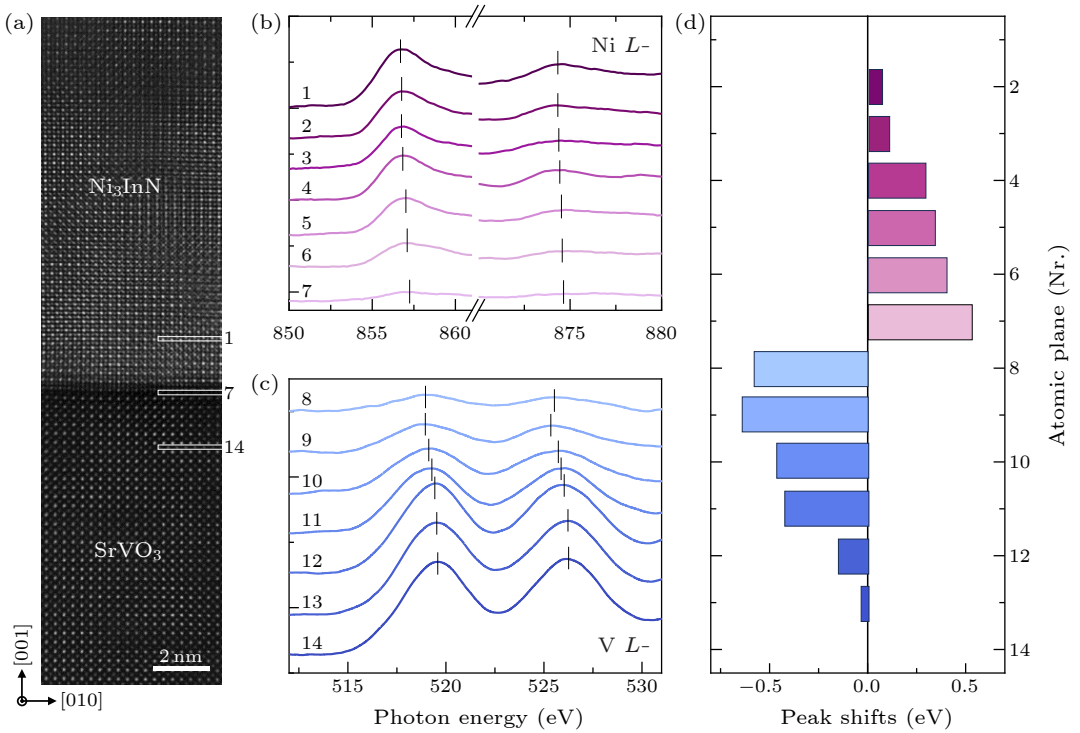

Fig. 2. Interfacial charge transfer at the $Ni_3InN/SrVO_3$ heterointerface. (a) HAADF-STEM image at the $Ni_3InN/SrVO_3$ interface region, with an EELS line scan across the interface. (b) and (c) EELS spectra at the Ni L- and V L-edges, respectively. The numbers in (a) represent the atomic layers across the interface. (d) Peak shifts of the EELS spectra as a function of atomic layers. The Ni L-edge peaks shift to higher energies, while the V L-edge peaks shift to lower energies moving from the bulk to the interface, indicating an increase in the valence states of Ni and a decrease in the valence states of V.

The high-resolution HAADF-STEM image at the interface region is shown in Fig. 2(a). Structural analysis demonstrated that the as-grown Ni_3InN thin films exhibit excellent crystallinity and a well-ordered antiperovskite structure with Ni ions in the face-center and N ions in the body-center. The interface between Ni_3InN and $SrVO_3$ is atomically sharp, consistent with the cube-on-cube epitaxy growth. EELS further confirms a distinct nitrogen signal within the Ni_3InN thin films. Our X-ray absorption spectra indicate a strong intensity at N K-edge, indicating the presence of N content. EELS results demonstrate the negligible chemical intermixing across the Ni_3InN and $SrVO_3$ interfaces. These results demonstrate the high crystalline quality and chemical integrity of the heterostructure, validating the robustness of the epitaxial growth of both layers.

3. Interfacial Charge Transfer from Ni to V Evidenced by Layer-Resolved EELS. To exploit the interfacial charge transfer across the $Ni_3InN/SrVO_3$ interface, we conducted a series of EELS line scans from the Ni_3InN layer to the $SrVO_3$ layer to investigate the layer-resolved electronic structure. The EELS spectra were acquired at both the Ni $L_{2,3}$- and V $L_{2,3}$-edges across the heterointerface. Figures 2(b) and 2(c) illustrate the evolution of the electronic structures of Ni and V, respectively. In addition to variations in spectral intensity, significant peak shifts were observed: the Ni $L_{2,3}$ peaks increased by ∼0.6 eV from the Ni_3InN layer to the interface, whereas the V $L_{2,3}$ peaks decreased by ∼0.8 eV from the $SrVO_3$ layer to the interface. Detailed comparisons of these peak shifts are presented in Fig. 2(d). These pronounced differences between the $SrVO_3$ and Ni_3InN layers reveal a clear interfacial charge transfer, with electrons transferring from the Ni_3InN layer to the $SrVO_3$ layer. The most significant peak shifts were observed near the interface region, with the extent of charge transfer diminishing gradually as each layer extended further fromthe interface. The charge-modified region was confined to a thickness of 2–3 unit cells, indicating that the charge transfer is highly localized.

DFT calculations were conducted to validate charge transfer at the $Ni_3InN/SrVO_3$ interface and analyze its electronic structure. First, we calculated the electronic and magnetic properties of $SrVO_3$. The V^{4+} ion exhibits a finite magnetic moment of $1\,\mu_B$/V, consistent with its $3d^1$ configuration. However, the energy difference between the ferromagnetic state and A-type antiferromagnetic state is very small, suggesting a low magnetic ordering temperature, if not zero, which aligns with the paramagnetic nature of $SrVO_3$ observed in our experiments. Next, we evaluated the formation energy (ΔE) of five possible interfacial configurations between Ni_3InN and $SrVO_3$ [Fig. S1 of the Supplementary Materials (SM)]. These are Ni_2N-SrO, Ni_2N-VO_2, NiIn-SrO, NiIn-VO_2, and NiIn-SrO. The corresponding ΔE values are 0.753, 0.005, 1.013, 0.923, and 0.820 eV, respectively. Among these configurations, the Ni_2N-VO_2 termination exhibited the lowest ΔE value, indicating it as the most stable interface configuration [Fig. 3(a)]. This theoretical prediction is in excellent agreement with our atomic-resolution HAADF-STEM imaging [Figs. 3(a) and S2].

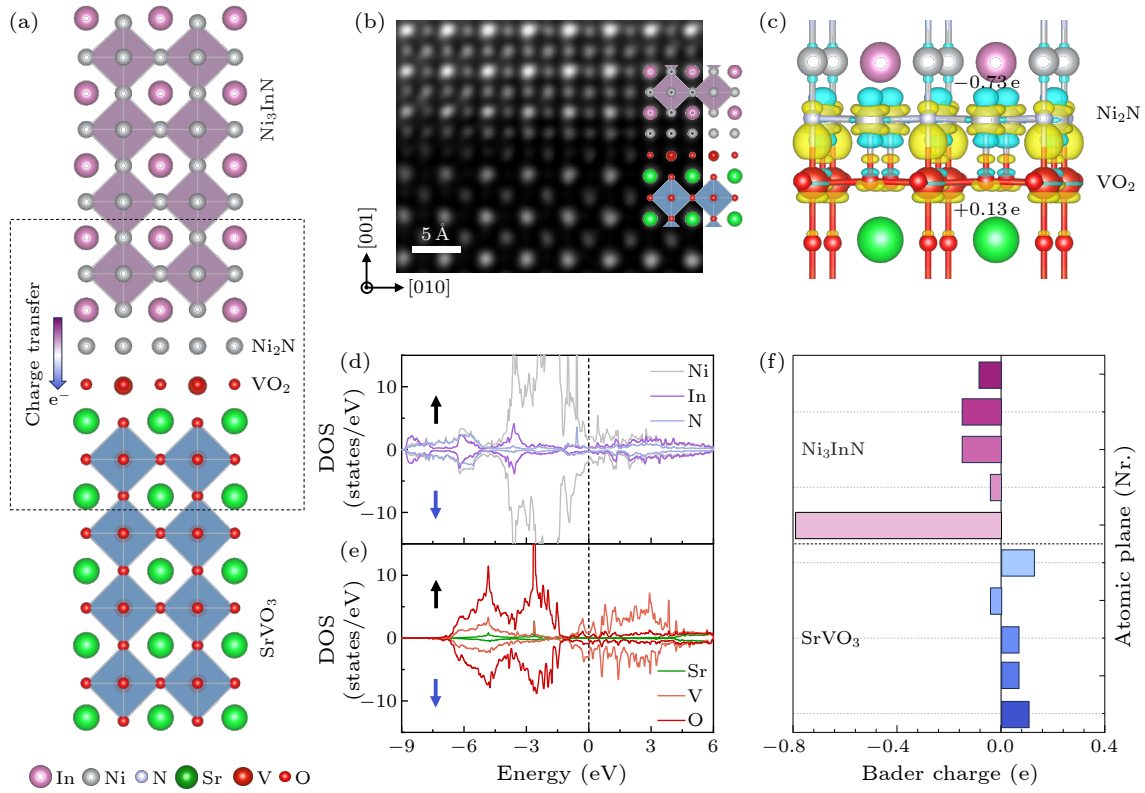

Fig. 3. First-principles calculations of the interfacial charge states and magnetism at the $Ni_3InN/SrVO_3$ interfaces. (a) Schematic illustration of the lowest-energy $Ni_3InN/SrVO_3$ interface with Ni_2N-VO_2 termination. (b) High-resolution HAADF-STEM image of the $Ni_3InN/SrVO_3$ heterostructure, confirming the Ni_2N-VO_2 interfacial configuration. (c) Electronic density difference distributions at the interface, with isosurfaces indicating electron accumulation (yellow) and charge depletion (blue), compared to the isolated Ni_3InN and $SrVO_3$ slabs. (d) and (e) Density of states (DOS) of the Ni_3InN and $SrVO_3$ layers with the Ni_2N-VO_2 configuration, respectively. The calculated DOS is shown with the Fermi level marked by the dashed line. The asymmetry between spin-up and spin-down state densities indicates the possible presence of magnetism in the $SrVO_3/Ni_3InN$ heterostructures. (f) Layer-resolved magnetic moment profile across the heterointerface.

To further confirm interfacial charge transfer, we performed charge density difference calculations across the $Ni_3InN/SrVO_3$ interface. Figure 3(c) presents the electronic density difference distributions at the interface, with isosurfaces indicating electron accumulation (yellow region) and charge depletion (blue region), compared to the isolated Ni_3InN and $SrVO_3$ slabs. Specifically, Ni atoms at the first interfacial layer exhibit electron depletion ($-0.73\,e$). Due to the broad spatial distribution of electron clouds in this metallic system, our DFT calculations provide semiquantitative rather than strictly quantitative values. Nonetheless, these results unambiguously confirm electron transfer from Ni_3InN to $SrVO_3$, in excellent agreement with our experimental observations.

Figures 3(d) and 3(e) present the density of states of Ni_3InN and $SrVO_3$, respectively. The results reveal substantial electron redistribution localized near the interface, with minimal changes in the bulk regions of both materials. As previously discussed, Ni ions in Ni_3InN adopt a low-spin state; however, magnetism can emerge under specific physical conditions. To further investigate the impact of interfacial coupling between the Ni_3InN and $SrVO_3$ layers, we examined the evolution of magnetic moments across atomic layers, as shown in Fig. 3(f). Remarkably, a strong local magnetic moment of $\sim 0.6\,\mu_B$/Ni emerges at the first interfacial Ni layer, despite the nominally nonmagnetic nature of bulk Ni_3InN. Concurrently, the local magnetic moment of V in $SrVO_3$ is enhanced from $\sim 1\,\mu_B$/V to $\sim 1.5\,\mu_B$/V at the first interfacial V layer. These interfacial moments exhibit an antiferromagnetic alignment between Ni and V, while the first two interfacial V layers become ferromagnetically coupled.

4. Discussions and Conclusions. The emergence of magnetism at the $Ni_3InN/SrVO_3$ interface is directly linked to the unconventional charge transfer across the heterostructure. In a typical oxide interface, charge transfer is primarily driven by band alignment and electrostatic potential differences. However, in this case, the presence of a Dirac-like metallic Ni_3InN layer with low-spin Ni ions creates an environment where charge redistribution can induce unexpected magnetic behavior. This unique behavior can be summarized in three aspects. Firstly, the electronic configuration of Ni has been modified by its bonding environment. In bulk Ni_3InN, Ni is in a low-spin state with a nominally nonmagnetic character due to strong hybridization between Ni 3d and N 2p orbitals. However, at the interface, electron depletion in the Ni layer ($\sim -0.73\,e$ per Ni_2N layer) disrupts this hybridization, shifting the

Ni 3d orbitals closer to an intermediate-spin or high-spin state. This results in the emergence of a localized magnetic moment at interfacial Ni sites, which is absent in bulk Ni_3InN. Secondly, the V magnetic moment in $SrVO_3$ enhances due to charge transfer. The electron accumulation at interfacial V sites ($\sim$+0.13 e per VO_2 layer) increases orbital occupancy and Coulomb interactions, reinforcing magnetic exchange interactions. The increased local moment suggests an interfacial-driven magnetic phase transition. Lastly, the induced Ni moments and enhanced V moments are antiferromagnetically coupled at the interface. This behavior resembles superexchange interactions in correlated electron systems where charge transfer modulates magnetic ordering. Additionally, the first two V layers exhibit ferromagnetic coupling, likely due to interface-mediated double exchange or kinetic energy stabilization.

In conclusion, we have fabricated a high-quality epitaxial heterostructure composed of antiperovskite nitride Ni_3InN and perovskite oxide $SrVO_3$. We demonstrate that the interfacial charge transfer near the $Ni_3InN/SrVO_3$ interface was confirmed through layer-resolved EELS and is consistent with our first-principles calculations. Unexpectedly, our findings reveal that charge transfer from Ni_3InN to $SrVO_3$ induces an unexpected magnetic moment within the Ni_3InN layer. These findings offer valuable insights into interfacial charge transfer mechanisms at nitride/oxide interfaces, highlighting their potential for next-generation electronic, magnetic, and energy applications.

Acknowledgements. This work was supported by the Beijing Natural Science Foundation (Grant No. JQ24002), the National Key Basic Research Program of China (Grant No. 2020YFA0309100), the National Natural Science Foundation of China (Grant Nos. U22A20263, 52250308, 12304158, 12325401, 12274069, 12404102, and 12474096), the Chinese Academy of Sciences (CAS) Project for Young Scientists in Basic Research (Grant No. YSBR-084), the CAS Youth Interdisciplinary Team, the Guangdong Basic and Applied Basic Research Foundation (Grant No. 2022B1515120014), the Guangdong-Hong Kong-Macao Joint Laboratory for Neutron Scattering Science and Technology, and the International Young Scientist Fellowship of Institute of Physics, CAS.

References

[1] Ohtomo A and Hwang H Y 2004 *Nature* **427** 423
[2] Cao C, Chen S, Deng J, Li G, Zhang Q, Gu L, Ying T P, Guo E J, Guo J G, and Chen X 2022 *Chin. Phys. Lett.* **39** 047301
[3] Cao Y, Wang Z, Park S Y, Yuan Y, Liu X, Nikitin S M, Akamatsu H, Kareev M, Middey S, Meyers D, Thompson P, Ryan P J, Shafer P, N'Diaye A, Arenholz E, Gopalan V, Zhu Y, Rabe K M, and Chakhalian J 2018 *Nat. Commun.* **9** 1547
[4] Lee H N, Christen H M, Chisholm M F, Rouleau C M, and Lowndes D H 2005 *Nature* **433** 395
[5] Liu K, Liu K, Zhang X, Fang J, Jin F, Wu W, Ma C, and Wang L 2024 *Chin. Phys. Lett.* **41** 117701
[6] Yi D, Liu J, Hsu S L, Zhang L, Choi Y, Kim J W, Chen Z, Clarkson J D, Serrao C R, Arenholz E, Ryan P J, Xu H, Birgeneau R J, and Ramesh R 2016 *Proc. Natl. Acad. Sci.* **113** 6397
[7] Zhao M, Chen A, Liu E, Zhao L, Wang S, He S, Zhang X, and Jiang W 2025 *Chin. Phys. Lett.* **42** 047502
[8] Gibert M, Zubko P, Scherwitzl R, Íñiguez J, and Triscone J M 2012 *Nat. Mater.* **11** 195
[9] Gibert M, Viret M, Zubko P, Jaouen N, Tonnerre J M, Torres-Pardo A, Catalano S, Gloter A, Stéphan O, and Triscone J M 2016 *Nat. Commun.* **7** 11227
[10] Fu Q, Zhou K, Chen L, Xu Y, Zhou T, Wang D, Chi K, Meng H, Liu B, Liu R, and Du Y 2020 *Chin. Phys. Lett.* **37** 117501
[11] Jin Q, Zhang Q, Bai H, Huon A, Charlton T, Chen S, Lin S, Hong H, Cui T, Wang C, Guo H, Gu L, Zhu T, Fitzsimmons M R, Jin K J, Wang S, and Guo E J 2023 *Adv. Mater.* **35** 2208221
[12] Jin Q, Wang Z, Zhang Q, Yu Y, Lin S, Chen S, Qi M, Bai H, Huon A, Li Q, Wang L, Yin X, Tang C S, Wee A T S, Meng F, Zhao J, Wang J O, Guo H, Ge C, Wang C, Yan W, Zhu T, Gu L, Chambers S A, Das S, Charlton T, Fitzsimmons M R, Liu G Q, Wang S, Jin K J, Yang H, and Guo E J 2022 *Phys. Rev. Lett.* **128** 017202
[13] Jin Q, Cheng H, Wang Z, Zhang Q, Lin S, Roldan M A, Zhao J, Wang J O, Chen S, He M, Ge C, Wang C, Lu H B, Guo H, Gu L, Tong X, Zhu T, Wang S, Yang H, Jin K J, and Guo E J 2021 *Adv. Mater.* **33** 2005920
[14] Quintela C X, Campbell N, Shao D F, Irwin J, Harris D T, Xie L, Anderson T J, Reiser N, Pan X Q, Tsymbal E Y, Rzchowski M S, and Eom C B 2017 *APL Mater.* **5** 096103
[15] Lu N, Ji A, and Cao Z 2013 *Sci. Rep.* **3** 3090
[16] Ji A, Li C, and Cao Z 2006 *Appl. Phys. Lett.* **89** 252120
[17] Hajiri T, Matsuura K, Sonoda K, Tanaka E, Ueda K, and Asano H 2021 *Phys. Rev. Appl.* **16** 024003
[18] Yu R, Weng H, Fang Z, Dai X, and Hu X 2015 *Phys. Rev. Lett.* **115** 036807
[19] Takenaka K and Takagi H 2005 *Appl. Phys. Lett.* **87** 261902
[20] Uehara M, Uehara A, Kozawa K, and Kimishima Y 2009 *J. Phys. Soc. Jpn.* **78** 033702
[21] Quintela C X, Song K, Shao D F, Xie L, Nan T, Paudel T R, Campbell N, Pan X, Tybell T, Rzchowski M S, Tsymbal E Y, Choi S Y, and Eom C B 2020 *Sci. Adv.* **6** eaba4017
[22] Nan T, Quintela C X, Irwin J, Gurung G, Shao D F, Gibbons J, Campbell N, Song K, Choi S Y, Guo L, Johnson R D, Manuel P, Chopdekar R V, Hallsteinsen I, Tybell T, Ryan P J, Kim J W, Choi Y, Radaelli P G, Ralph D C, Tsymbal E Y, Rzchowski M S, and Eom C B 2020 *Nat. Commun.* **11** 4671
[23] Cao Y, Yang Z, Kareev M, Liu X, Meyers D, Middey S, Choudhury D, Shafer P, Guo J, Freeland J W, Arenholz E, Gu L, and Chakhalian J 2016 *Phys. Rev. Lett.* **116** 076802
[24] Colby R, Qiao L, Zhang K H L, Shutthanandan V, Ciston J, Kabius B, and Chambers S A 2013 *Phys. Rev. B* **88** 155325
[25] Gibert M, Viret M, Torres-Pardo A, Piamonteze C, Zubko P, Jaouen N, Tonnerre J M, Mougin A, Fowlie J, Catalano S, Gloter A, Stéphan O, and Triscone J M 2015 *Nano Lett.* **15** 7355
[26] Jang H W, Felker D A, Bark C W, Wang Y, Niranjan M K, Nelson C T, Zhang Y, Su D, Folkman C M, Baek S H, Lee S, Janicka K, Zhu Y, Pan X Q, Fong D D, Tsymbal E Y, Rzchowski M S, and Eom C B 2011 *Science* **331** 886
[27] Ohtomo A, Muller D A, Grazul J L, and Hwang H Y 2002 *Nature* **419** 378
[28] Wang L, Yang Z, Koirala K P, Bowden M E, Freeland J W, Sushko P V, Kuo C T, Chambers S A, Wang C, Jalan B, and Du Y 2024 *Sci. Adv.* **10** eadq6687
[29] Yu L and Zunger A 2014 *Nat. Commun.* **5** 5118

[30] Shao Z, Fu Z G, Li S, Cao Y, Bian Q, Sun H, Zhang Z, Gedeon H, Zhang X, Liu L, Cheng Z, Zheng F, Zhang P, and Pan M 2019 *Nano Lett.* **19** 5304
[31] Chen M, Ning X, Hu X, Sun J, Fu N, Li Y, Wang J, Wang S, and Fu G 2017 *Adv. Mater. Interfaces* **4** 1700252
[32] Cao L, Zhou G, Wu Q, Yang S A, Yang H Y, Ang Y S, and Ang L K 2020 *Phys. Rev. Appl.* **13** 054030
[33] Hoffman J D, Kirby B J, Kwon J, Fabbris G, Meyers D, Freeland J W, Martin I, Heinonen O G, Steadman P, Zhou H, Schlepütz C M, Dean M P M, te Velthuis S G E, Zuo J M, and Bhattacharya A 2016 *Phys. Rev. X* **6** 041038
[34] Lee S, Lee A T, Georgescu A B, Fabbris G, Han M G, Zhu Y, Freeland J W, Disa A S, Jia Y, Dean M P M, Walker F J, Ismail Beigi S, and Ahn C H 2019 *Phys. Rev. Lett.* **123** 117201
[35] Zhang Y, Shinokita K, Watanabe K, Taniguchi T, Goto M, Kan D, Shimakawa Y, Moritomo Y, Nishihara T, Miyauchi Y, and Matsuda K 2020 *Adv. Mater.* **32** 2003501
[36] Omar G J, Li M, Chi X, Huang Z, Lim Z S, Prakash S, Zeng S, Li C, Yu X, Tang C, Song D, Rusydi A, Venkatesan T, Pennycook S J, and Ariando A 2020 *Nano Lett.* **20** 2493
[37] Moyer J A, Eaton C, and Engel-Herbert R 2013 *Adv. Mater.* **25** 3578
[38] Cao W H, He B, Liao C Z, Yang L H, Zeng L M, and Dong C 2009 *J. Solid State Chem.* **182** 3353